Biochimica et Biophysica Acta 1787 (2009) 635–645

Contents lists available at ScienceDirect

Biochimica et Biophysica Acta

journal homepage: www.elsevier.com/locate/bbabio

High resolution crystal structure of *Paracoccus denitrificans* cytochrome *c* oxidase: New insights into the active site and the proton transfer pathways

Juergen Koepke, Elena Olkhova, Heike Angerer, Hannelore Müller, Guohong Peng, Hartmut Michel *

Max Planck Institute of Biophysics, Department of Molecular Membrane Biology, Max-von-Laue-Str.3, D-60438 Frankfurt/Main, Germany

ARTICLE INFO

Article history:
Received 12 February 2009
Received in revised form 3 April 2009
Accepted 8 April 2009
Available online 15 April 2009

Keywords:
Electron transfer
Proton transfer
Proton pumping
X-ray crystallography
Membrane protein structure

ABSTRACT

The structure of the two-subunit cytochrome *c* oxidase from *Paracoccus denitrificans* has been refined using X-ray cryodata to 2.25 Å resolution in order to gain further insights into its mechanism of action. The refined structural model shows a number of new features including many additional solvent and detergent molecules. The electron density bridging the heme a_3 iron and Cu_B of the active site is fitted best by a peroxo-group or a chloride ion. Two waters or OH^- groups do not fit, one water (or OH^-) does not provide sufficient electron density. The analysis of crystals of cytochrome *c* oxidase isolated in the presence of bromide instead of chloride appears to exclude chloride as the bridging ligand. In the D-pathway a hydrogen bonded chain of six water molecules connects Asn131 and Glu278, but the access for protons to this water chain is blocked by Asn113, Asn131 and Asn199. The K-pathway contains two firmly bound water molecules, an additional water chain seems to form its entrance. Above the hemes a cluster of 13 water molecules is observed which potentially form multiple exit pathways for pumped protons. The hydrogen bond pattern excludes that the Cu_B ligand His326 is present in the imidazolate form.

1. Introduction

Cytochrome *c* oxidase (CcO) is the terminal enzyme of the respiratory chains of mitochondria and of many aerobic prokaryotes. It uses electrons from cytochrome *c* to reduce molecular oxygen (dioxygen) to water and couples this reaction to the pumping of four protons across the membrane (for reviews see [1–3]). The different origin of the four protons consumed in water formation (from the cytoplasmic side of prokaryotes or from the mitochondrial matrix) and that of the electrons (from the external side), as well as the pumping of four protons generates a difference of the electrochemical potential of protons. This electrochemical potential gradient across the membrane is used by the adenosine 5′-triphosphate synthase by coupling the backflow of protons to the generation of ATP from ADP and inorganic phosphate.

The structures of three "canonical" CcOs, namely from the soil bacterium *Paracoccus* (*P.*) *denitrificans* [4,5], from bovine heart mitochondria [6,7] and from the purple bacterium *Rhodobacter* (*Rb.*) *sphaeroides* [8,9] have been determined by X-ray crystallography. Subunit II of CcO binds the Cu_A centre, which is reduced by cytochrome *c* from the external, periplasmic surface. Subsequently the electron is transferred to heme *a*, and then to the heme a_3/Cu_B binuclear site. Molecular oxygen (dioxygen) is supposed to bind to the heme a_3 iron, when both the heme iron and Cu_B are reduced after transfer of a second electron. Heme *a*, heme a_3 and Cu_B are located in the hydrophobic interior of the enzyme at the same height, but closer to the external surface than to the internal surface (see also Fig. 1). The protons required for water formation during the catalytic cycle therefore have to travel through more than half of the membrane. Based on the X-ray crystallographic structure determinations and on prior mutagenesis experiments [10,11] two proton transfer pathways have been identified. The K-pathway, named after its essential lysine residue Lys354, leads straight into the active site. It appears to be used only for one or two protons during the initial reduction of the oxidized enzyme, whereas the residual six or seven protons travel through the so-called D-pathway [12]. All pumped protons appear to use this longer pathway which leads from the highly conserved aspartate Asp124 to another highly conserved residue, glutamic acid Glu278. Because also two or three of the consumed protons use the D-pathway, protons have to be transferred from Glu278 either to the propionates of heme a_3 [4] or further to His326, which has been postulated to be in the imidazolate form in the oxidized enzyme and to be the proton acceptor for protons waiting to be pumped [13,14]. The pumping itself is then caused by electrostatic repulsion from another proton which enters the binuclear site and is consumed there in the chemical reaction. Such pumping mechanisms (see e.g. [15] for discussion) are based on electrostatic repulsion in accordance with Peter Rich's electroneutrality principle [16] stating that each electron transfer into the hydrophobic interior of CcO is charge compensated by the uptake of a proton. This charge compensating proton originates from the internal surface and is not consumed in the chemical

* Corresponding author.
E-mail address: michel@mpibp-frankfurt.mpg.de (H. Michel).

0005-2728/$ – see front matter © 2009 Elsevier B.V. All rights reserved.
doi:10.1016/j.bbabio.2009.04.003

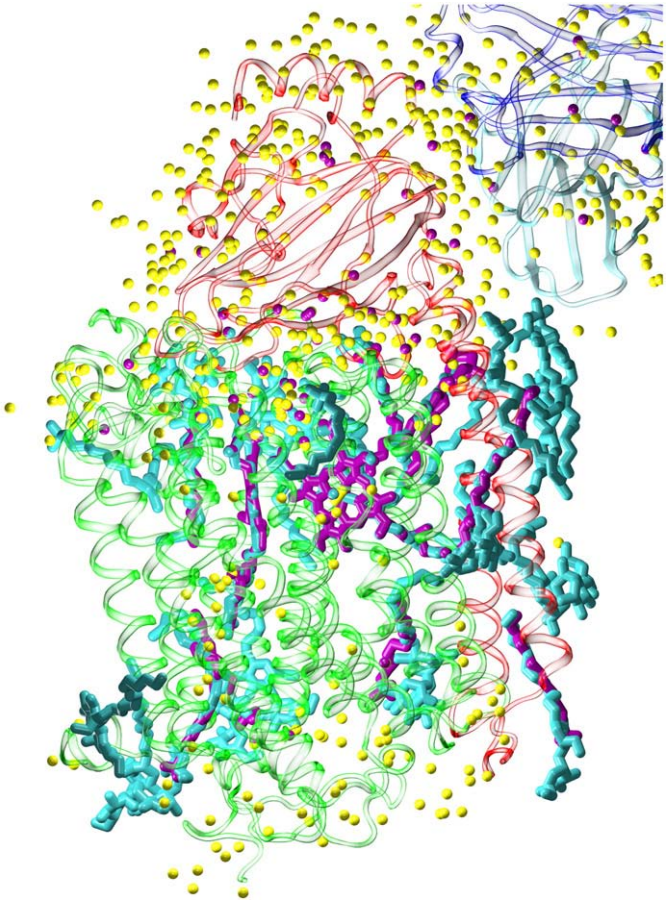

Fig. 1. Superposition of the structures obtained with data collected at 4 °C (protein data base entry 1AR1) or with cryo-cooled crystals (this work). The protein structure is shown in new cartoon representation, with subunit I colored in light green, subunit II in red and the two Fv fragment subunits in blue. Prosthetic groups and detergent molecules of the cryo-cooled structure are shown in cyan, while water molecules are colored in yellow. Non-protein atoms of the 4 °C structure are shown in magenta. Thus, in comparing yellow and magenta spheres it becomes obvious, the number of refined water molecules has increased considerably when cryo-cooling the measured crystal. The software used for visualization was VMD [54].

reactions at the active site. The active site of the fully oxidized CcO contains a Fe^{+III} (real charge +1) and a Cu^{2+} ion. Because of the close distance (4.59 Å) a negatively charged bridging ligand is required to prevent electrostatic repulsion between the two positively charged metal ions. In addition, both have unpaired electrons in their 3d orbitals, they are antiferromagnetically coupled and require a bridging ligand between each other [17].

For the bovine heart enzyme it has been published that a chloride ion might be bridging the two metal ions in the active site of the oxidized CcO, when the enzyme is purified in the presence of this anion [18]. This "resting" enzyme has to be activated by reduction, which is supposed to lead to proton uptake, and release of the chloride as HCl and replacement by an OH^- during turnover. However, in bacterial CcOs such resting states (see [19] for a review) are ill characterized or may be even absent [20].

Proton translocation in proteins is supposed to occur along hydrogen bonded chains, by shifting the proton from the hydrogen bond donor to the hydrogen bond acceptor successively along the chain. Hydrogen bonded water molecules as well as amino acid side chains can contribute to such a so-called "proton wire". For a fast and efficient proton transfer each hydrogen bond donor also has to accept a hydrogen bond at the same time. However, gaps in the hydrogen bonded chains might be bridged by reorientations of amino acid side chains with p*K* values appropriate to release and to accept protons. Examples are Glu278 in the D-pathway or Lys354 in the K-pathway.

In this publication we present the refined structure of the wild type two-subunit CcO from *P. denitrificans* complexed with an Fv fragment of a monoclonal antibody. Data could be collected using frozen crystals to a resolution of 2.25 Å, a considerable increase in resolution compared to the structure measured at 277 K [5]. Many new items could be added. In the following we put the emphasis on the results of a careful refinement of the active, binuclear site as well as of the proton transfer pathways.

2. Materials and methods

2.1. Purification and crystallization of cytochrome c oxidase

At the beginning wild type *P. denitrificans* cells were used which had been grown in a fermenter (GBF Braunschweig, kindly provided by Prof. B. Ludwig, University of Frankfurt). Crystals of CcO isolated from these cells diffracted to less than 3 Å resolution. Later crystals of CcO variants were obtained diffracting to a considerably higher resolution. Therefore "wild type" CcO was prepared using the same homologous expression system as used for the production of CcO variants. The wild type gene (isoform 2) of the *Paracoccus* CcO subunit I was cloned into the vector pUP39 [21]. The plasmid transfer into *P. denitrificans* was performed by triple mating using the *P. denitrificans* strain AO1 [22] and the *Escherichia coli* helper strain RP4-4. *P. denitrificans* wild type cells were grown in succinate medium as described [21]. The two-subunit CcO was purified via the Fv fragment 7E2 [23] and crystallized as described [5]. In order to investigate whether a suspected chloride might be present in the active site of the isolated enzyme, several CcO preparations were made using buffers where all chloride had been replaced by equimolar amounts of bromide. In addition, dithionite was added to these CcO preparations (to fully reduce CcO) and air-oxidized again three times prior to the final ion exchange chromatography step. The enzyme as isolated and crystallized has a Soret band absorption maximum at 424–425 nm which is typically for the fast or pulsed forms of CcO (see [19] for review). It is highly likely that the crystallized CcO becomes reduced during the X-ray crystallographic data collection at the synchrotron. However, due to the temperature around 100 K it is unlikely that the reduction leads to subsequent structural changes.

2.2. X-ray data collection, processing, and refinement

The crystals were cryo-protected with 25% (v/v) glycerol and flash-frozen in a stream of a gaseous cryo-stream cooled by liquid nitrogen. X-ray diffraction data were collected using synchrotron beamline X10SA (PXII) of the Swiss Light Source in Villigen, Switzerland. The two data sets collected were indexed and processed with the program XDS [24] to a resolution of 2.25 or 2.5 Å, respectively. Data collection statistics are listed in Table 1. Compared to the crystals used for collecting data at 277 K for the structure determination of CcO from *P. denitrificans* [5] (protein data base (PDB) entry 1AR1), a considerable shrinking in one unit cell dimension (*a*-axis) was observed. Therefore the structure had to be determined employing the Molecular Replacement Method using the native model 1AR1 in the program EPMR [25]. Refinement of the data against the accordingly rotated and translated 1AR1 model was started with CNS [26] employing the rigid body and annealing protocol. Later refinement was switched to Refmac5 [27], with structure factors calculated from the measured intensities using TRUNCATE of the CCP4 suite of programs [28]. Between each refinement round $2F_o–F_c$ electron density maps and $F_o–F_c$ difference-density maps were inspected utilizing the graphics program XtalView [29]. To detect firmly bound water molecules the solvent structure building routine of ARP/wARP [30] was applied. Alternatively, detergent molecules have been

Table 1
Data collection statistics.

Dataset	1AR1	3HB3	Wild-type 2	1V54	1M56
Species	*Paracoccus denitrificans*			Bovine	*Rb. sphaeroides*
Unit cell					
a[Å]	93.53	83.40	84.01	182.59	340.4
b[Å]	151.04	150.47	151.07	205.14	340.4
c[Å]	156.70	157.19	158.15	178.25	89.7
Spacegroup	$P2_12_12_1$				R3
Resolution [Å]	2.7	2.25 (2.35–2.25)	2.5 (2.6–2.5)	1.8	2.3 (2.9–2.7)[b], (2.4–2.3)[a]
R_{symm} [%]	7.4	12.4 (37.9)	9.6 (37.4)		7.9 (37)[b], (79)[a]
Multiplicity	2.05	4.9 (4.9)	7.4 (7.2)		1.9 (2.8)[b], (2.5)[a]
Completeness [%]	98.4	99.0 (98.3)	97.8 (97.1)		69.3 (70.0)[b], (36.0)[a]
I/σ (*I*)		14.2 (3.2)	19.2 (3.4)		8.6 (3.5)[b], (1.5)[a]
R_{free} (*R*) [%]	23.5 (20.1)	28.0 (21.8)	26.7 (22.4)	22.7 (20.2)	27.5 (23.6)
Rmsd					
Bond [Å]		0.031	0.018		0.012
Angle [°]		2.683	2.011		
Solvent molecules	63	579	501	2006	448
Water	54	555	480	1970	436
LDAO[c]	9	10	7		
LMT[d]		14	14		
PEH[e]					12

[a] Numbers in parenthesis are values for the highest resolution shell.
[b] Numbers in parenthesis are values for the second highest resolution shell.
[c] Lauryl dimethylamine oxide.
[d] Lauryl-β-D-maltoside.
[e] Di-stearoyl-3-sn-phosphatidylethanolamine.

fitted to difference-density peaks in the membrane region of cytochrome *c* oxidase instead of water molecules. Since lauryl-β-D-maltoside has been exchanged against lauryl-*N*,*N*-dimethylamine-*N*-oxide during purification, both detergent molecules were found. The quality of the electron density at 1.0σ can be inspected in Fig. 2, where the electron density of the active site is shown. Distances between metal centers and their coordinating side chains or internal water molecules, where restrained during refinement to values found in the Refmac5 [26] libraries, while for the crosslink between $N_{\varepsilon 2}$ of His 276 and $C_{\varepsilon 2}$ of Tyr 280 [5,7] the backbone N–C_α distance for prolines of 1.468 Å was chosen [31].

3. Results

3.1. Newly added features

Because of the higher resolution new electron density appeared which allowed the addition of 501 additional water and 15 detergent molecules (see Table 1). Whereas in our old structure (PDB entry 1AR1) the electron density attributable to detergents molecules were exclusively modeled as lauryl-*N*,*N*-dimethylamine-*N*-oxides we have now added 14 lauryl-β-D-maltosides, several of them replacing lauryl-*N*,*N*-dimethylamine-*N*-oxides because electron density for the polar maltoside head group showed up. In Fig. 1 our new structure using data collected under cryo-conditions to 2.25 Å resolution and the structure based on data collected at 277 K to a resolution of 2.7 Å (PDB entry 1AR1) are superimposed. The increase in solvent molecules is evident. The 277 K structure contains e.g. no water molecules in the cytosolic half of CcO. In the new structure several new water molecules are visible in the membrane spanning part. Most of them are part of proton transfer pathways (see below).

Table 1 also compares the data collection and refinement statistics for the structures of "canonical" CcOs which contain water molecules in the deposited coordinates.

3.2. Active site

Table 2 shows important distances and bond angles characterizing the active site around the heme a_3 iron and Cu_B and compares the values deposited for other CcO structures in the Protein Data Bank. Only the lower resolved bovine CcO coordinate set 2OCC was deposited together with its bound substrate. The two lower resolution structures 1AR1 and 1M56 (*Rb. sphaeroides*) were obviously refined without restraining the distance of the covalent crosslink between $N_{\varepsilon 2}$ of His 276 and $C_{\varepsilon 2}$ of Tyr 280. The two *P. denitrificans* coordinate sets show the shortest distances between the iron and copper atoms. However, the original structure of the four-subunit CcO *P. denitrificans* [4,32] (PDB entry 1QLE), shows a longer distance of 5.15 Å, comparable to the other ones in Table 2. The shorter distance might be due to the fact that the crystals of the two-subunit CcO from *P. denitrificans* were obtained at rather low pH values around 5.5 in contrast to the other crystals. The central heme a_3 iron is out of the plane, defined by the central nitrogen atoms of the porphyrin ring system, in most structures as can be deduced from the merged bond angles Heme N–Fe–His N. Only in the structure presented here and the PDB entries 1M56 and 2OCC is this angle close to 90° and thus the iron in plane with the ring system.

The observed electron density bridging the iron and Cu_B in the active site might be caused by the presence of a single water molecule or one OH^- ion, two distinct water molecules or OH^- ions, one water molecule and one OH^- ion, dioxygen, a peroxide (dianion), a hydrogen carbonate ion, or a Cl^- ion. To discriminate between these possibilities a careful refinement has been done. The situation with two oxygen atoms not restrained in the O–O distance is shown in Fig. 2a. Two oxygen atoms are refined to a distance of only 1.64 Å. Thus the two oxygen atoms are far too close to belong to different molecules even when they were hydrogen bonded. Please note that the shortest hydrogen bond in the Cambridge small molecule data base [33] has a length of 2.4 Å. This result also appears to exclude that the bridging electron is caused by two OH^- ions, two water molecules or one water molecule plus one OH^- ion, even when they are hydrogen bonded. Dioxygen shows an O–O distance of 1.085 Å, while in a peroxide the two oxygen atoms should be 1.474 Å apart. A refinement of an oxygen molecule in this place resulted in an O–O distance of 1.12 Å and for a peroxide of 1.51 Å. Refining one single water molecule (or one OH^- ion) instead, produces a 5.0σ difference-density peak at the position of the missing oxygen (Fig. 2b). The difference-density peak gives a clear indication, where a second oxygen atom should be located. To refine a HCO_3^- ion in the active site was only possible by constraining

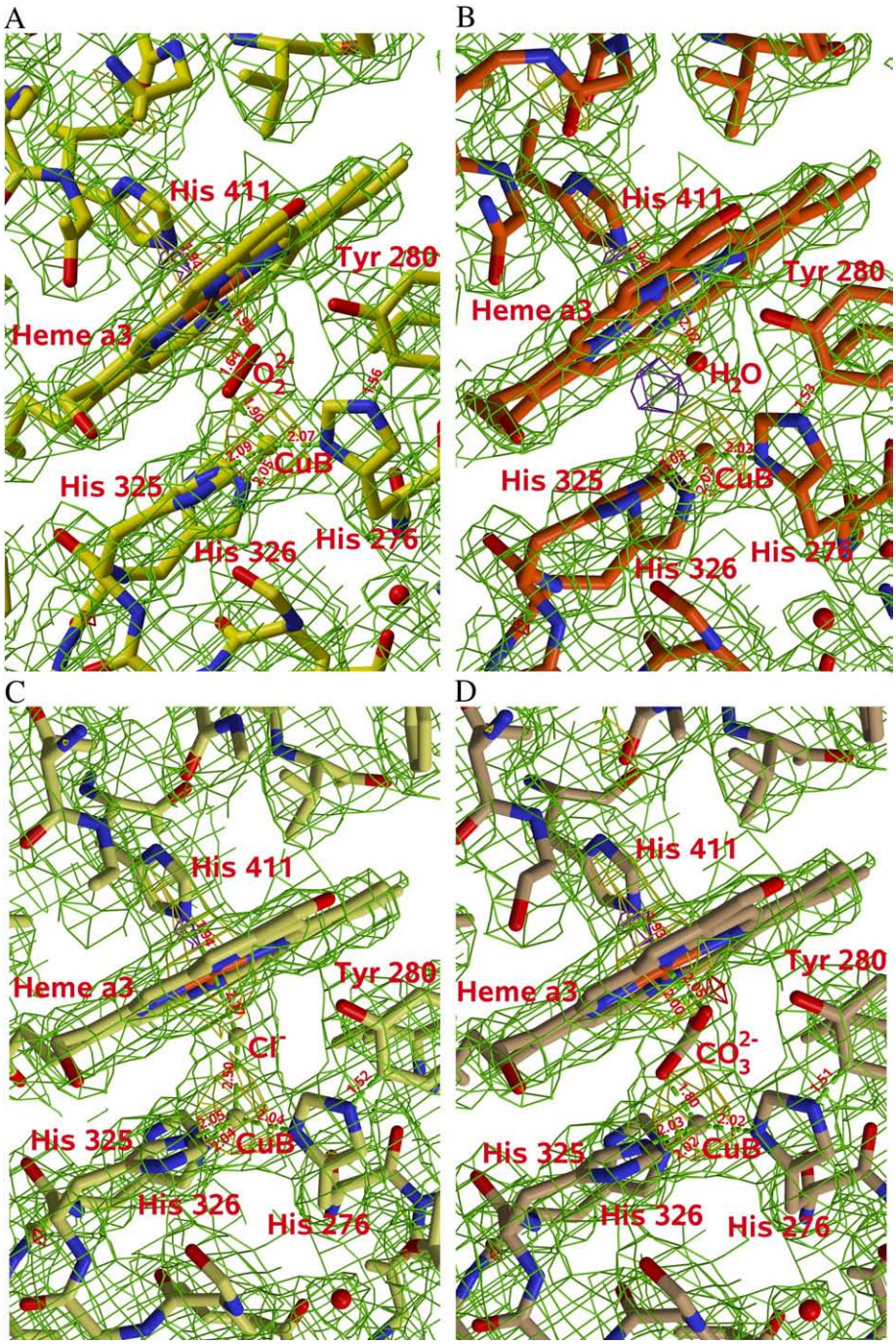

Fig. 2. (A) Active site model refined with two independent oxygen atoms bound to the heme a_3 iron and the Cu_B, respectively. The refined O–O distance of 1.64 Å fits best to a peroxide molecule bridging the two metal centres, but is too short for a distinct water molecule and an OH^- ion, the reason for the two oxygen atoms to be connected by the red bond in the drawing. Active site with only (B) a single water molecule, (C) a Cl^- anion, and (D) a CO_3^{2-} anion refined between the metal centres. $2F_o–F_c$ Electron density at 1.0σ of the active site in wireframe representation colored in green. Additionally in yellow the 5.0σ level and at ±4.0σ the $F_o–F_c$ difference density is shown in magenta and red, respectively. The molecular models are drawn with balls and sticks, color coded according to their atom type. Coordination distances for heme a_3 Fe and Cu_B are indicated by dashed green lines, with their respective lengths given in Å. Visible is also the crosslink between His276 $N_{\varepsilon 2}$ and Tyr280 $C_{\varepsilon 2}$. No difference density above or below 4.0σ is observable in the vicinity of the two models shown in a and c of this figure, thus no decision between O_2^{2-} and Cl^- is possible alone from the diffraction data. While b and d show either a positive or negative difference density, indicating either, in case of a single water molecule, a deficit or, in case of the HCO_3^- anion, an excess of the refined model, respectively.

one oxygen atom to be bound to the copper and the two others to the iron. A small difference electron density of 4.0σ remains in this case close to one of the oxygens bound to the heme a_3 iron (Fig. 2c). Hydrogen carbonate as a bridging ligand therefore appears to be excluded. Finally a good fit to the bridging electron density is obtained with a Cl^- ion (Fig. 2d). The anion refines closer to the iron (distance Fe–Cl^-: 2.17 Å, Cu–Cl^-: 2.50 Å), but probably the resolution of 2.25 Å is not sufficient to accurately place a Cl^- ion between two much stronger scatterers. As a result both a peroxide (dianion) and a chloride can explain the bridging electron density. In order to obtain further hints which alternative is correct, CcO from *P. denitrificans* was isolated in the presence of bromide instead of chloride. Bromide is expected to replace a bound chloride, in particular upon turnover of CcO when a bound chloride is supposed to leave the resting enzyme as hydrogen chloride. No difference electron density between bromide and chloride data, nor an

Table 2
Dimensions of the active site in cytochrome *c* oxidases.

Dataset	1AR1	3HB3	1M56	1V54	1V55	2OCC	1OCR
	Oxidized	Oxidized	Oxidized	Oxidized	Reduced	Oxidized	Reduced
Resolution [Å]	2.7	2.25	2.7/2.3	1.8	1.9	2.3	2.35
Fe–Cu [Å]	4.46	4.62	4.82	4.99	5.13	4.85	5.13
Crosslink distance [Å]	2.66	1.52	2.46	1.37	1.37	1.36	1.35
Heme N–Fe [Å]	1.96	2.13	1.94	2.02	2.01	1.95	1.99
His N–Fe [Å]	2.15	1.94	2.24	2.04	2.19	1.91	1.86
His N–Cu [Å]	2.18	2.02	2.09	2.00	1.99	2.01	2.32
Heme N–Fe–His N [°]	102.3	92.9	89.5	96.3	97.8	91.5	97.9

anomalous difference signal caused by a bridging bromide could be detected. This result therefore might favor a peroxide bridge between the heme a_3 iron and Cu_B.

3.3. Proton translocation pathways

3.3.1. D-pathway

The D-pathway starts at Asp124 close to the cytoplasmic surface of CcO. Asp124 is connected by a single water molecule to Asn131. Inside a cavity between Asn131 and Glu278 eleven internal water molecules could be localized. Six of them form a linear chain of hydrogen bonded water molecules connecting Asn131 and Glu278. The electron density for one water molecule adjacent to Asn 131 is rather week (0.3σ) and its hydrogen bond distance of 3.54 Å to the next water in the chain is long. In the structure of CcO from bovine heart (PDB entry 1V54, ref. [34]) the two corresponding water molecules are separated by 2.78 Å and in the *Rb. sphaeroides* CcO (PDB entry 1M56, ref. [8]) by 3.05 Å. In Fig. 3 parts of subunit I forming the D-pathway of the PDB entries 1V54 and 1M56, and the *P. denitrificans* wild type structure presented here have been superimposed together with their visible water molecules (note that the numbering of the corresponding residues is shifted by −36 for the bovine enzyme and by +8 for the *Rb. sphaeroides* CcO). Corresponding water molecules of the D-pathway could be easily detected. Differences in the water positions between the *P. denitrificans* CcO and bovine CcO are observed in the central part, while close to Glu278 (corresponding to Glu242 in bovine CcO) no water molecules are visible in bovine CcO in contrast to the *P. denitrificans* CcO. The water chain in *Rb. sphaeroides* CcO resembles that of the *P. denitrificans* CcO much better but contains gaps (Fig. 3). Gaps are also seen when the data of the second crystal of *P. denitrificans* CcO (Wild-type 2 in Table 1), diffracting only to 2.5 Å resolution, have been used thus confirming that the number of detected internal water molecules is resolution dependent. However, one fundamental difference between the hydrogen bond patterns around the *P. denitrificans* Asn131 and the corresponding bovine Asn98 on one hand and the corresponding *Rb. sphaeroides* Asn139 on the other hand is that in the model of the *Rb. sphaeroides* CcO the side chain amide NH_2 separates two water molecules, whereas in the *P. denitrificans* and bovine CcOs both the amide NH_2 and the amide carbonyl oxygen interrupt the water chain. This important difference is discussed below.

3.3.2. K-pathway

In the K-pathway only two internal water molecules have been found consistently in all three high resolution CcO X-ray structures. One water molecule is hydrogen bonded to the OH group of the hydroxyethylfarnesyl side chain of heme a_3 and to Thr351, the other one links Ser291 and the essential Lys354 after which the K-pathway has been named (see Fig. 4a). It is under debate which residues form the entrance to the K-pathway. Originally electrostatic long range interactions have been found between the binuclear active site and Glu78(II) of subunit II [35]. As a consequence the corresponding Glu101(II) of the *Rb. sphaeroides* CcO has been mutated. The resulting CcO variants were found to resemble classical K-pathway variants leading to the conclusion that Glu101 (II) may form the entry to the K-pathway [36]. However, the corresponding variants in *P. denitrificans* showed wild type activity [37] excluding that in *P. denitrificans* Glu78(II) has a similar role as the essential Asp124 at the entrance of the D-pathway. In the present *P. denitrificans* CcO structure we found electron density for

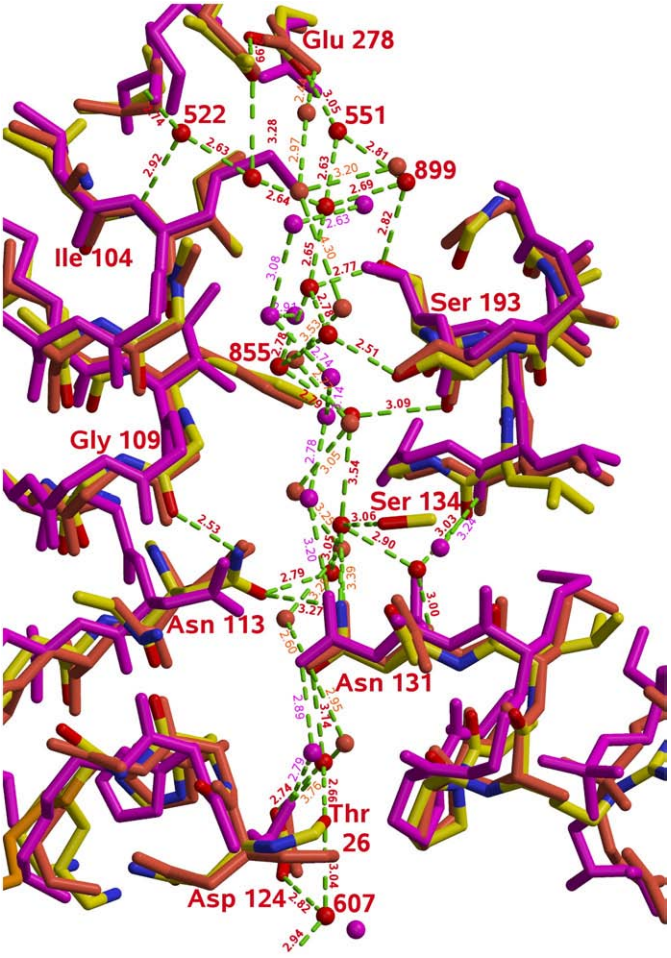

Fig. 3. Superposition of the structure of cytochrome *c* oxidase from bovine heart (PDB entry 1V54), shown in magenta, and from *Rb. sphaeroides* (PDB entry 1M56), shown in orange, onto the *P. denitrificans* wild type structure of this work, by using corresponding residues shifted either −36 or +8 in numbering, respectively. Putative hydrogen bonds between water molecules accounting for a water chain along the D-pathway are represented by dashed green lines with their respective length given in Å and color coded like the atomic model. Only the water molecules of this work are connected all the way between the two residues Asn131 and Glu278. The water chain of the *Rb. sphaeroides* CcO shows two distances of 4.30 and 3.76 Å, too long for a hydrogen bond, while the water chain of bovine heart is not connected to Glu242, corresponding to Glu278 in *P. denitrificans*.

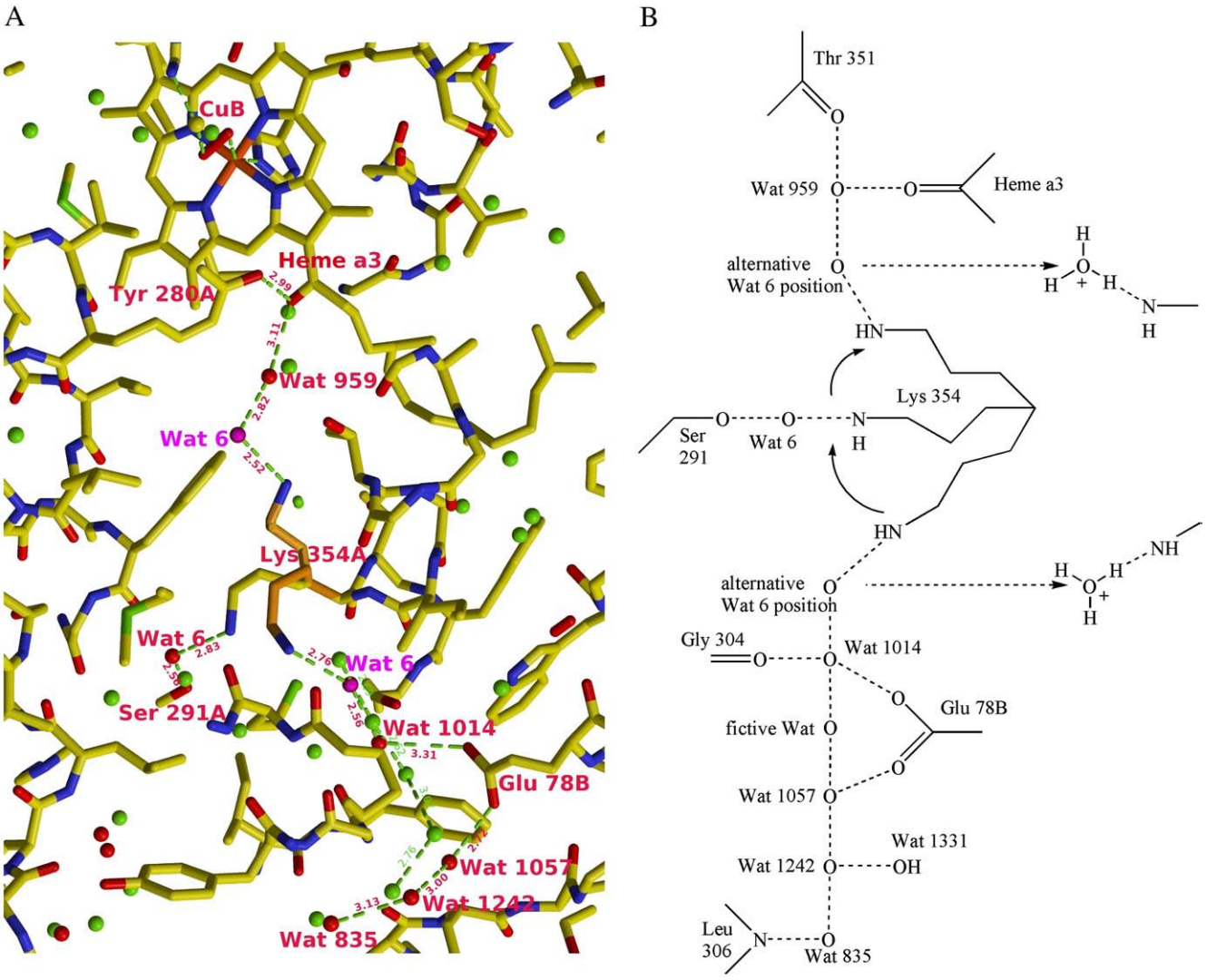

Fig. 4. (A) Superposition of water molecules from a molecular dynamics simulation in green onto the *P. denitrificans* wild type structure. For the side chain of Lys 354 three orientations are shown. In the X-ray structure the side chain is oriented towards Ser 291, while the other two orientations shown in orange are hypothetical orientations necessary for proton transfer along the K-pathway. Wat 6 also shown in three positions participates in the hypothetical movement of the lysine. The two hypothetical water orientations are shown in magenta. Hydrogen bonds between water molecules accounting for a water chain along the K-pathway are represented by dashed green lines with their respective length given in Å and color coded like the atomic model. (B) Water structure of the K-pathway in a schematic drawing. Lysine 354 is shown in 2 putative orientations together with possible positions of water 6, to demonstrate the movement of this residue. Between the two water molecules 1014 and 1057, which bind to Glu78(II), a water molecule was added to complete the water chain as in the molecular dynamics simulation [38].

four water molecules close to Glu78(II). Two of these are hydrogen bonded to Glu78(II). They are in positions nearly identical to respective members of a water chain, placed into the *P. denitrificans* CcO structure on the basis of energy minimizations [38]. However, the modeled chain of water molecules is more complete than the one observed in the electron density (see Fig. 4a) and may well form the entry for protons into the K-pathway without a direct involvement of Glu78(II). The side chain of Lys354 is observed in a position also found in other X-ray structures and probably trapped in an orientation pointing towards Ser 291 by a bridging water molecule.

3.3.3. Exit pathways

The water cluster located above heme a_3 is connected directly via hydrogen bonds to the Mg^{2+}/Mn^{2+} site and its ligands (Fig. 5a). Altogether 13 water molecules, of which three coordinate the Mg^{2+}/Mn^{2+} atom, constitute the cluster. His326, one of the three histidine ligands to Cu_B of the binuclear center, is in hydrogen bond distance to water 7 (Fig. 5b), and appears to be hydrogen bonded also to the δ-propionate and the α-propionate of heme a_3 as well as to water 949. The cluster undergoes further hydrogen bonds to the α- and δ-propionates of heme a_3, to arginines 473 and 474, to Glu218(II), Thr329, and Asp399. The side chain of Asp193(II) (corresponding to bovine Asp173B(II)) is in hydrogen bonding distance to two water molecules coordinating the Mg^{2+}/Mn^{2+} site. His326 is of particular interest because it has been proposed to be the "pump loading site" of CcO [13,14], this means that protons to be pumped are stored at the side chain of His326. In this case the side chain of His326 has to be in the imidazolate form in oxidized CcO. Asp173(II) and Lys171(II) of bovine CcO have been proposed [39] to be the most probable exit point for the proton exit pathway. However, Fig. 5a and b show several viable alternatives. Arginines 473 and 474 which form salt bridges to the δ-propionates of heme a_3 and heme *a*, respectively, have been proposed to be the entrance to the proton exit channel [40]. However, variants with mutations of the corresponding residues in the *Rb. sphaeroides* CcO retain substantial proton pumping activity [41].

From the water cluster several water chains emerge towards the periplasmic side beginning e.g. at either Lys191(II), Arg400, or Arg474. The water chain starting close to Arg474 is directly connected via a hydrogen bond to the water cluster, while the two others lack such a

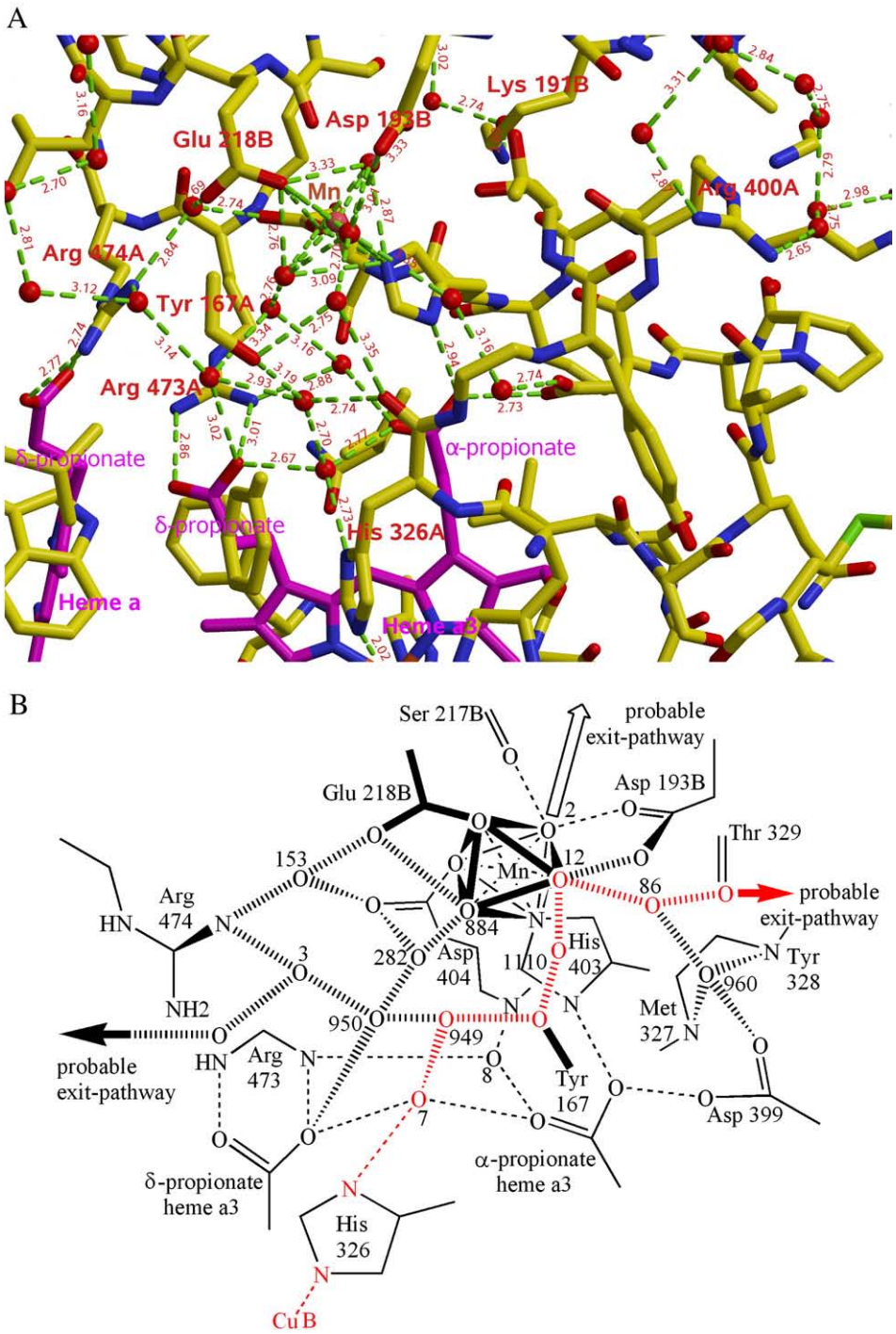

Fig. 5. (A) Hydrogen bond network of the water cluster above heme a_3. Hydrogen bonds are represented by dashed green lines with their respective length given in Å. The coordination octahedron around the Mg^{2+}/Mn^{2+} site is indicated by additional dashed lines, connecting the ligands. Carbon atoms of the hemes *a* and a_3 are colored magenta to distinguish them from the protein atoms. There exists no distinct exit pathway, but several choices might be possible. Close to Arg474, Asp139 of subunit II, and Arg 400 water chains are visible, which are connected to the outside water molecules. (B) Schematic drawing of the water cluster above heme a_3 in the exit pathways. Residues and water molecules in a higher level are indicated by thicker lines of its bonds. A probable proton pathway through the cluster was highlighted in red color, but other paths, to other exits are possible as well. Water molecules are only indicated by their number.

direct link. Lys191(II) with its flexible side chain might bridge the gap by side chain rotation.

4. Discussion

4.1. Structure of the active site

The precise structure of the active site of CcO, in particular the nature of the ligand(s) between the heme a_3 iron and Cu_B, is still under debate. Old models of the catalytic cycle of CcO did not consider this question. However, it is evident that two positively charged metal ions cannot be in close contact without (an) intervening negatively charged ligand(s) because of the otherwise strong electrostatic repulsion between the metal ions. With the advent of the X-ray structures of CcOs which showed the presence of an electron density bridging the heme a_3 iron and Cu_B the discussion about the nature of the intervening ligand has been intensified. The electron density between the heme a_3 iron and Cu_B has been interpreted as being due

to a bridging peroxide dianion in case of the bovine enzyme [7], whereas for the *P. denitrificans* CcO an OH^- ligand bound to Cu_B and possibly a water molecule bound to the heme a_3 iron was favored [5]. On the basis of the results presented here we discard the possibility of the presence of both a water bound to heme a_3 iron and an OH^- to Cu_B because there is simply not enough space and because the distance of about 4.6 Å between the two metal ions is too short for fitting two oxygen atoms which should have a distance of about 1.8 to 2 Å each to the metal ions and an hydrogen bond of more than 2.4 Å between them. The distance between two refined oxygen positions of 1.64 Å is also too long for molecular dioxygen, but it is in good agreement with a peroxide molecule bridging the heme a_3 iron and Cu_B as first proposed by Yoshikawa et al. [7]. In addition, it has also been noted for the *Rb. sphaeroides* CcO that a peroxide provides the best fit for the electron density between heme a_3 iron and Cu_B [9], but this finding was not discussed further. We therefore face the situation that for all the canonical CcOs of known structure the best fit is provided by a peroxide! Only for the aberrant ba_3 type CcO from *Thermus thermophilus* the electron density between the heme a_3 iron and Cu_B was refined as being due to a single oxygen atom species (μ-oxo, OH^- or water) [42].

As mentioned above a Cl^- ion would provide a perfect fit for the bridging electron density. However, our numerous attempts to exchange chloride against bromide by replacing in all buffers chloride by bromide, reducing the CcO and reoxiding it again during the purification procedure several times, crystallization of the CcO and data collection close to the bromo K absorption edge (0.9198 Å) did not provide any hint for the presence of chloride instead of bromide in the active site. We therefore have to consider the possibility of chloride being the bridging ligand as unlikely.

Are there other arguments in favor of a peroxide in the binuclear site? In the oxidized CcO the heme iron has a formal charge of +III, but a real charge of +1 only, because the central heme iron replaces two protons of the porphyrin system, whereas Cu_B has a real charge of +2. Therefore a bridging peroxide dianion is much better suited than a single OH^- ligand for electrostatically compensating the positive charges on both metal ions. A charge compensation by two OH^- ligands, one at Cu_B, the other one at the heme a_3 iron, is unlikely because there is insufficient space between the heme iron and Cu_B to accommodate both of them. Synthetic organic chemists have put a lot of successful efforts in synthesizing functional chemical mimics of the active site of CcOs (for review see [43–45]). In particular, such mimics contain a peroxide dianion bridging the Fe^{+III} and Cu_B^{+2} [46–48]. The peroxide dianion is converted into a superoxide monoanion upon reduction of the Cu_B^{+2} mimic [46]. These properties of the functional mimics clearly support the existence of a peroxide dianion in the oxidized state of CcO. For the bovine CcO it has been postulated that the peroxide bridge is present only in the resting state of the oxidized enzyme but not in the enzyme because a hydroxide bound to the heme a_3 iron has been detected by resonance Raman spectroscopy (see e.g. [49]) in the late part of the catalytic cycle. However, the signal for this hydroxyl intermediate disappears on the few millisecond time scale [49]. It is therefore possible that the OH^- ligand is replaced by a bridging peroxide in the cycle. Having a peroxide in the resting state of the enzyme would pose the additional question about its origin.

4.2. Proton transfer pathways

Our study has confirmed that hydrogen bonded water molecules may be part of all proton transfer pathways, in particular the D-pathway is lined up with water molecules. A close inspection reveals that a number of open important problems exist which rarely have been addressed. We shall start with discussing features of the D-pathway. Asp124 is located close to the protein surface at the cytoplasmic side. It is then connected to the side chain of Asn131 by hydrogen bonds donated by a connecting water molecule (Fig. 6a and b, water 622). This bridging water molecule can be predicted to be a donor of a hydrogen bond to Asp124, because Asp124 is most likely deprotonated as predicted from the results of electrostatic calculations [50] in agreement with the results of Fourier transform infrared spectroscopy (P. Hellwig, personal communication). The side chain carbonyl oxygen of Asn131 is most likely the hydrogen bond acceptor for the bridging water molecule, because the side chain amide nitrogen provides of Asn131 donates a hydrogen bond to the side chain carbonyl oxygen of Asn113 whose side chain amide nitrogen in turn donates a hydrogen bond to the backbone carbonyl oxygen of Gly109 (see Fig. 6a, b). The side chain amide nitrogen of Asn131 then provides a hydrogen bond to a member of the continuous hydrogen bonded water chain which leads up to Glu278. Asn131 is surrounded by Asn199 and Asn113. Apart from one predicted water molecule [38] (see Fig. 6b) connecting the side chain carbonyl oxygen atoms of Asn113 and Asn131 there appears to be no space for a productive uninterrupted hydrogen bonded chain from water 622 to the water chain connecting Asn131 and Asn199 to Glu278 (see Fig. 6b). On the contrary, the three asparagines seem to form an effective block for proton transfer. It appears to be impossible to transfer a proton from water 622 to water 972. The p*K* values of the asparagine side chains seem to exclude the possibility that the side chain carbonyl oxygen or the side chain amide nitrogen becomes protonated and that a proton is carried over by a side chain rotation. The hydrogen bond pattern at the entrance to the D-pathway as described here is very similar in the CcOs of *P. denitificans* and from bovine mitochondria excluding the possibility of proton transfer through the D-pathway in the oxidized enzymes. One has to note that a blocked D-pathway in oxidized CcO is in agreement with the finding that proton uptake upon reduction of heme *a* in the oxidized *P. denitificans* CcO occurs through the K-pathway [51]. Inspection of the deposited coordinates (PDB entry code 1M56) for the *Rb. sphaeroides* [8] CcO suggests that the situation in the *Rb. sphaeroides* CcO may be different because the side chain amide nitrogen (Asp139 in *Rb. sphaeroides*) there directly links two water molecules. As a result the amide nitrogen might receive a proton from the equivalent to Wat 622 and deliver a proton to the next water in the chain. However, one has to realize that the data statistics for *Rb. sphaeroides* CcO structure indicates that the data are of very low quality beyond 2.7 Å resolution and overall less than 70% complete. Therefore it is an open question whether there is a real difference in the hydrogen bond pattern around Asp131 (Asp139) between the *Rb. sphaeroides* CcO and the two other CcOs or the difference is an artifact due to the lower resolution and data quality of the *Rb. sphaeroides* CcO.

We localized a total of eleven water molecules in the cavity between Asn131 and Glu278. However, one should mention here, that an unrestrained refinement of the water positions led to unrealistically short hydrogen bond distances in the upper part of the D-pathway. This result might be connected to the postulated storage of an excess proton in the upper part of the D-pathway [52]. Six of the water molecules form a chain directly connecting the residues Asn131 and Glu278, but the remaining water molecules may have an important role as well (Fig. 6a, b). A whole network of hydrogen bonded water molecules and hydrogen bond donating residues might be necessary to create a sufficient solvation shell for the proton being translocated. Molecular modeling studies [38] show even more water molecules in the water filled cavities of the protein, which support the notion, that more water molecules participate directly or indirectly in the proton translocation, besides the very rigid structural water molecules identified by X-ray crystallography. This statement must be particularly true for the proton transfer pathways connecting Glu278 to the pump loading site and to the binuclear center. No water molecules being part of these pathways could be located.

Because Asp124 appears to be deprotonated its role deserves further discussion. In its deprotonated form it cannot be a productive member of a proton transferring hydrogen bonded chain. Its role may be more indirect, its negative charge may be required to polarize the

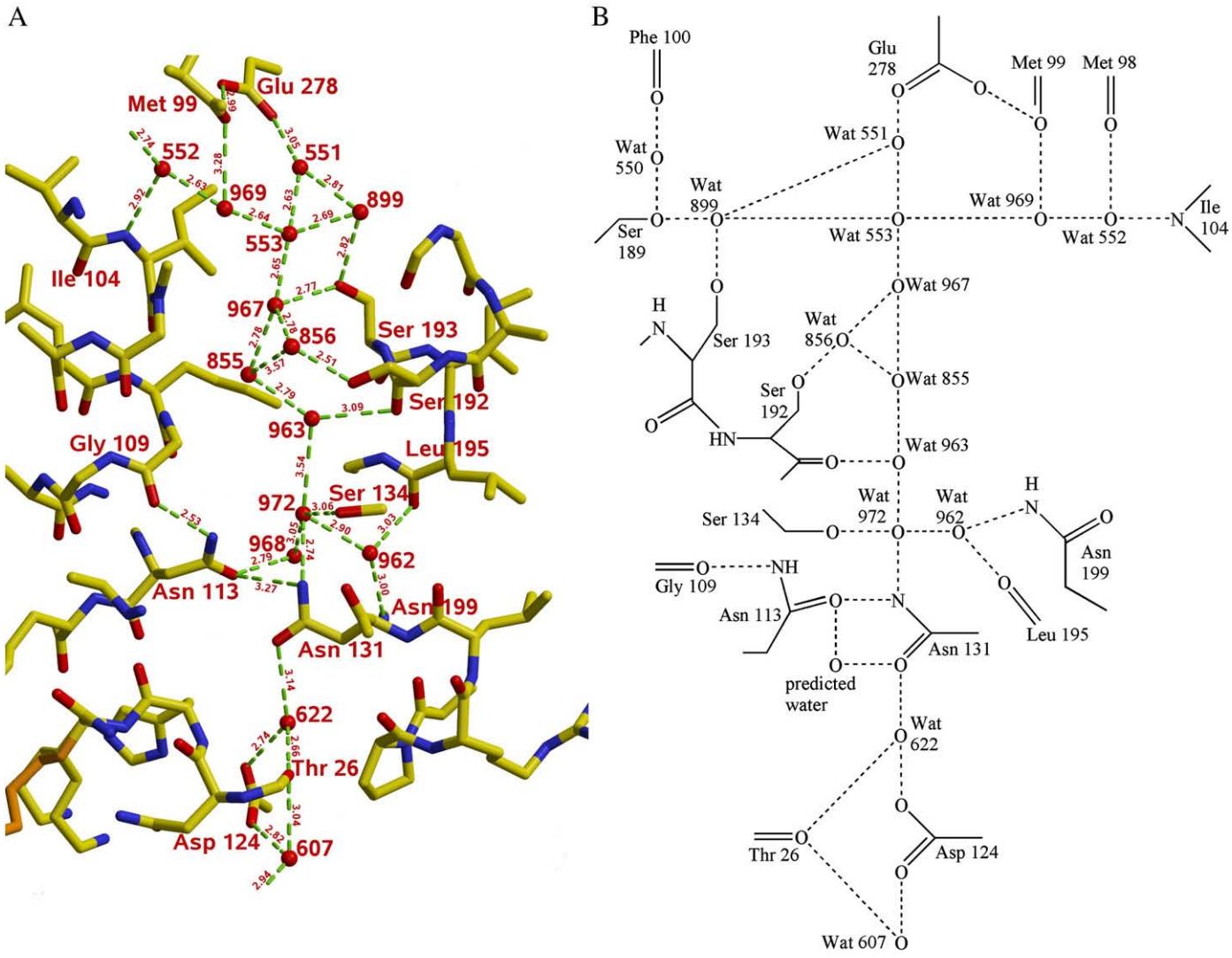

Fig. 6. (A) View onto the water molecules of the D-pathway. Six molecules in the cavity between Asn131 and Glu278 form a hydrogen bonded chain connecting both residues. Two additional water molecules connect the chain to Asn113 and Asn199. Another water molecule bridges Asn131 and Asp124, responsible for the name of the pathway. At the entrance of the pathway a small chain of two water molecules is visible connecting the pathway to the bulk water. Hydrogen bonds are represented by dashed green lines with their respective length given in Å. (B) Water structure of the D-pathway in a schematic drawing. One water position was added, placed as in a molecular dynamics simulation [38].

hydrogen bonded chain in the right direction. A hydrogen bonded chain would be unable to transfer protons towards Glu278 if the members of the chain would donate their hydrogen bonds downwards to the member further away from Glu278. For an efficient proton transfer towards Glu278 the polarity of the hydrogen bonded chain has to be the opposite, the members of the chain have to donate hydrogen bonds upwards to the chain members closer to Glu278. The negative charge at Asp124 is well suited to enforce the correct polarity of the hydrogen bonded chain to enable efficient proton transfer.

Close to the entrance to the K-pathway there are four water molecules connected directly or indirectly as a hydrogen bonded chain to Glu78(II). The water placement for the molecular dynamics simulation shows where additional water molecules could complete the chain (Fig. 4b) and allow entry of protons into the K-pathway. This water chain allows bypassing Glu78(II), the role of this residue therefore would be to support and fix the water chain. As mentioned, the experimental results between *Rb. sphaeroides* and *P. denitrificans* differ; the homologous residue is essential in *Rb. sphaeroides*, but not in *P. denitrificans* [36,37]. Mutations of this residue might disrupt the water chain and therefore block proton conduction in one organism, but not in the other. The central, name providing residue Lys354 has been found in the same position in all high resolution CcO X-ray structures in hydrogen bond distance to a water which is hydrogen bonded to Ser291. In this position it is not connected to the water chain around Glu78(II). However, there is enough space for alternative side chain conformations (see Fig. 4a). It might rotate to water 6 in an alternative position contacting the water chain around Glu78(II) as modeled in Fig. 4a, pick up a proton, rotate further into an upward conformation and deliver a proton towards water 959, from there a productive hydrogen bonded chain consisting of the hydroxy group of the hydroxyethylfarnesyl side chain of heme a_3 and the phenolic OH group of Tyr280 exists.

In the region above the hemes and Cu_B, a water cluster of 13 internal water molecules has been found (Fig. 5b). This water cluster must be connected to the “pump loading site” on one hand and contribute to the exit pathway for protons on the other. Distinct exit pathways for protons and water molecules were proposed [39]. One water chain to the outer surface emerges close to the arginines 473 and 474 is connected to Wat 3 of the cluster. Inside the cluster several paths exist, which connect the heme a_3 propionates and His326, a ligand of Cu_B, to the Mg^{+2}/Mn^{+2} site. The heme propionates (e.g. [15]) as well as His326 [13,14] have been proposed to be the pump loading site. Both alternative pump loading sites are connected and the exit pathways can be reached. Two other probable exit pathways

can be reached from the cluster via Wat 2, a ligand of the Mg^{+2}/Mn^{+2} ion, and via Wat 12 and Wat 86. The proposal that His326 is the pump loading site [53] is difficult to reconcile with the hydrogen bond pattern of Fig. 5b: His326 is hydrogen bonded to Wat 7, which undergoes further hydrogen bonds with both heme a_3 propionates as well as with another water molecule. The α-propionate however shares a proton with Asp399 and can therefore not be a donor of a hydrogen bond to water 7. The δ-propionate forms an ion pair with Arg473 (or hydrogen bonds if a proton would be transferred from Arg473 to the δ-propionate, or shared between them) and can also not be a hydrogen bond donor to water 7. Therefore both heme propionates are acceptors of hydrogen bonds from water 7. Water 7 then cannot donate a hydrogen bond to His326, but only be a hydrogen bond acceptor. It is a consequence of this observed hydrogen bond pattern that the side chain of His326 must be a donor of a hydrogen bond and therefore be in its neutral imidazole form. As such it is unlikely that it serves as the pump loading site.

5. Conclusions

The careful X-ray crystallographic refinement of the structure and the analysis of the electron density in the active site of the *P. denitrificans* CcO led to the conclusion that a peroxide dianion and chloride provide the best fit for the electron density between the heme a_3 iron atom and Cu_B. Because bromide, expected to replace chloride when present in excess in the absence of chloride, does not cause a change of this electron density, and there is no anomalous signal, it is most likely that this electron density is caused by the presence of a peroxide (dianion) bridging the heme a_3 iron atom and Cu_B. The negative charges of a peroxide dianion also would provide an excellent charge compensation for the positive charges of the two metal ions.

The D-pathway of proton transfer appears to be blocked by the side chains of a cluster of three asparagines close to its entrance in the oxidized form of CcO. Multiple pathways do exist for the exit of pumped protons. An analysis of the hydrogen bond pattern around the heme propionates strongly suggests that the side chain of His326, proposed to be present in the negatively charged imidazolate form and to be the "pump loading site", is in the neutral imidazole form. This finding appears to exclude that it serves as the pump loading site.

6. PDB Accession Code

The 2.25 Å resolution structure was deposited with accession code 3HB3 in the Protein Data Bank.

References

[1] R.B. Gennis, Coupled proton and electron transfer reactions in cytochrome oxidase, Frontiers in Bioscience 9 (2004) 581–591.
[2] P. Brzezinski, G. Larsson, Redox-driven proton pumping by heme-copper oxidases, Biochim. Biophys. Acta (BBA) – Bioenergetics 1605 (2003) 1–13.
[3] H. Michel, J. Behr, A. Harrenga, A. Kannt, Cytochrome *c* oxidase: structure and spectroscopy, Annu. Rev. Biophys. Biomol. Struct. 27 (1998) 329–356.
[4] S. Iwata, C. Ostermeier, B. Ludwig, H. Michel, Structure at 2.8 Å resolution of cytochrome *c* oxidase from *Paracoccus denitrificans*, Nature 376 (1995) 660–669.
[5] C. Ostermeier, A. Harrenga, U. Ermler, H. Michel, Structure at 2.7 Å resolution of the *Paracoccus denitrificans* two-subunit cytochrome *c* oxidase complexed with an antibody Fv fragment, Proc. Natl. Acad. Sci. U. S. A. 94 (1997) 10547–10553.
[6] T. Tsukihara, H. Aoyama, E. Yamashita, T. Tomizaki, H. Yamaguchi, K. Shinzawa-Itoh, R. Nakashima, R. Yaono, S. Yoshikawa, The whole structure of the 13-subunit oxidized cytochrome *c* oxidase at 2.8 Å, Science 272 (1996) 1136–1144.
[7] S. Yoshikawa, K. Shizawa-Itho, R. Nakashima, R. Yaono, E. Yamashita, N. Inoue, M. Yao, M.J. Fei, C. Peters-Libeu, T. Mizushima, H. Yamaguchi, T. Tomizaki, T. Tsukihara, Redox-coupled crystal structural changes in bovine heart cytochrome *c* oxidase, Science 280 (1998) 1723–1729.
[8] M. Svensson-Ek, J. Abramson, G. Larsson, S. Tornroth, P. Brezezinski, S. Iwata, The X-ray crystal structures of wild-type and Eq(I-286) mutant cytochrome *c* oxidases from *Rhodobacter sphaeroides*, J. Mol. Biol. 321 (2002) 329–339.
[9] L. Qin, C. Hiser, A. Mulichak, R.M. Garavito, S. Ferguson-Miller, Identification of conserved lipid/detergent-binding sites in a high-resolution structure of the membrane protein cytochrome *c* oxidase, Proc. Natl. Acad. Sci. U. S. A. 103 (2006) 16117–16122.
[10] J.W. Thomas, A. Puustinen, J.O. Alben, R.B. Gennis, M. Wikstrom, Substitution of asparagine for aspartate-135 in subunit I of the cytochrome bo ubiquinol oxidase of *Escherichia coli* eliminates proton-pumping activity, Biochemistry 32 (1993) 10923–10928.
[11] J.A. Garcia-Horsman, A. Puustinen, R.B. Gennis, M. Wikstrom, Proton transfer in cytochrome bo3 ubiquinol oxidase of *Escherichia coli*: second-site mutations in subunit I that restore proton pumping in the mutant Asp135→Asn, Biochemistry 34 (1995) 4428–4433.
[12] A.A. Konstantinov, S. Siletsky, D. Mitchell, A. Kaulen, R.B. Gennis, The roles of the two proton input channels in cytochrome *c* oxidase from *Rhodobacter sphaeroides* probed by the effects of site-directed mutations on time-resolved electrogenic intraprotein proton transfer, Proc. Natl. Acad. Sci. U. S. A. 94 (1997) 9085–9090.
[13] J. Quenneville, D.M. Popović, A.A. Stuchebrukhov, Redox-dependent pK_a of Cu_B histidine ligand in cytochrome *c* oxidase, J. Phys. Chem. B 108 (2004) 18383–18389.
[14] D.M. Popoviç, A.A. Stuchebrukhov, Proton pumping mechanism and catalytic cycle of cytochrome *c* oxidase: Coulomb pump model with kinetic gating, FEBS Lett. 566 (2004) 126–130.
[15] H. Michel, Cytochrome *c* oxidase: catalytic cycle and mechanism of proton pumping — a discussion, Biochemistry 38 (1999) 15129–15140.
[16] P.R. Rich, Towards an understanding of the chemistry of oxygen reduction and proton translocation in the iron–copper respiratory oxidases, Australian J. Plant Physiol. 22 (1995) 479–486.
[17] G. Palmer, G.T. Babcock, L.E. Vickery, A model for cytochrome oxidase, Proc. Natl. Acad. Sci. U. S. A. 73 (1976) 2206–2210.
[18] E. Forte, M.C. Barone, M. Brunori, P. Sarti, A. Giuffre, Redox-linked protonation of cytochrome *c* oxidase: the effect of chloride bound to Cu_B, Biochemistry 41 (2002) 13046–13052.
[19] A.J. Moody, "As prepared" forms of fully oxidised haem/Cu terminal oxidases, Biochim. Biophys. Acta 1276 (1996) 6–20.
[20] S.E. Brand, S. Rajagukguk, K. Ganesan, L. Geren, M. Fabian, D. Han, R.B. Gennis, B. Durham, F. Millett, A new ruthenium complex to study single-electron reduction of the pulsed O_H state of detergent-solubilized cytochrome oxidase, Biochemistry 46 (2007) 14610–14618.
[21] U. Pfitzner, K. Hoffmeier, A. Harrenga, A. Kannt, H. Michel, E. Bamberg, O.M.H. Richter, B. Ludwig, Tracing the D-pathway in reconstituted site-directed mutants of cytochrome *c* oxidase from *Paracoccus denitrificans*, Biochemistry 39 (2000) 6756–6762.
[22] U. Pfitzner, A. Odenwald, T. Ostermann, L. Weingard, B. Ludwig, O.M.H. Richter, Cytochrome *c* oxidase (heme aa_3) from *Paracoccus denitrificans*: analysis of mutations in putative proton channels of subunit I, J. Bioenerg. Biomembr. 30 (1998) 89–97.
[23] G. Kleymann, C. Ostermeier, B. Ludwig, H. Michel, Engineered Fv fragments as a tool for the one-step purification of integral multisubunit membrane–protein complexes, Bio/Technology 13 (1995) 155–160.
[24] W. Kabsch, Automatic processing of rotation diffraction data from crystals of initially unknown symmetry and cell constants, J. Appl. Cryst. 26 (1993) 795–800.
[25] C.R. Kissinger, D.K. Gehlhaar, D.B. Fogel, Rapid automated molecular replacement by evolutionary search, Acta Cryst. D55 (1999) 484–491.
[26] A.T. Brünger, P.D. Adams, G.M. Clore, W.L. DeLano, P. Gros, R.W. Grosse-Kunsleve, J.S. Jiang, J. Kuszewski, M. Nilges, N.S. Pannu, R.J. Read, L.M. Rice, T. Simonson, G.L. Warren, Crystallography and NMR system: a new software suite for macromolecular structure determination, Acta Cryst. D54 (1998) 905–921.
[27] G.N. Murshudov, A. Lebedev, A.A. Vagin, K.S. Wilson, E.J. Dodson, Efficient anisotropic refinement of macromolecular structures using FFT, Acta. Cryst. D55 (1999) 247–255.
[28] Collaborative Computing Project, Number 4, The *CCP*4 suite: programs for protein crystallography, Acta Cryst. D50 (1994) 760–763.
[29] D.E. McRee, Practical Protein Crystallography, Academic Press, 1999.
[30] S. Lamzin, A. Perrakis, K.S. Wilson, The ARP/wARP suite for automated construction and refinement of protein models, in: M.G. Rossmann, E. Arnold (Eds.), International Tables for Crystallography. Volume F: Crystallography of Biological Macromolecules, Dordrecht, Kluwer Academic Publishers, The Netherlands, 2001, pp. 720–722.
[31] R.A. Engh, R. Huber, in: M.G. Rossmann, E. Arnold (Eds.), International Tables for Crystallography, *Vol. F*, Dordrecht: Kluwer Academic Publishers, 2001, pp. 382–416.
[32] A. Harrenga, H. Michel, The cytochrome *c* oxidase from *Paracoccus denitrificans* does not change the metal center ligation upon reduction, J. Biol. Chem. 274 (1999) 33296–33299.
[33] F.H. Allen, The Cambridge Structural Database: a quarter of a million crystal structures and rising, Acta Cryst. B58 (2002) 380–388.
[34] T. Tsukihara, K. Shimokata, Y. Katayama, H. Shimada, K. Muramoto, H. Aoyama, M. Mochizuki, K. Shinzawa-Itoh, E. Yamashita, Y. Ishimura, S. Yoshikawa, The low-spin heme of cytochrome *c* oxidase as the driving element of the proton-pumping process, Proc. Natl. Acad. Sci. U. S. A. 100 (2003) 15304–15309.
[35] A. Kannt, C.R. Lancaster, H. Michel, The coupling of electron transfer and proton translocation: electrostatic calculations on *Paracoccus denitrificans* cytochrome *c* oxidase, Biophys. J. 74 (1998) 708–721.
[36] M. Bränden, F. Tompson, R.B. Gennis, P. Brezezinski, The entry point of the K-proton-transfer pathway in cytochrome *c* oxidase, Biochemistry 41 (2002) 10794–10798.
[37] O.M.H. Richter, K.L. Dürr, A. Kannt, B. Ludwig, F.M. Scandurra, A. Giuffre, P. Sarti, P. Hellwig, Probing the access of protons to the K pathway in the *Paracoccus denitrificans* cytochrome *c* oxidase, FEBS J. 272 (2005) 404–412.

[38] E. Olkhova, M.C. Hutter, M.A. Lill, V. Helms, H. Michel, Dynamic water networks in cytochrome *c* oxidase from *Paracoccus denitrificans* investigated by molecular dynamics simulations, Biophys. J. 86 (2004) 1873–1889.
[39] M.D. Popoviç, A.A. Stuchebrukhov, Proton exit channels in bovine cytochrome *c* oxidase, J. Phys. Chem. B 109 (2005) 1999–2006.
[40] A. Puustinen, M. Wikström, Proton exit from the heme-copper oxidase of *Escherichia coli*, Proc. Natl. Acad. Sci. U. S. A. 96 (1999) 35–37.
[41] J. Qian, D.A. Mills, L. Geren, K. Wang, C.W. Hoganson, B. Schmidt, C. Hiser, G.T. Babcock, B. Durham, F. Millett, S. Ferguson-Miller, Role of the conserved arginine pair in proton and electron transfer in cytochrome *c* oxidase, Biochemistry 43 (2004) 5748–5756.
[42] T. Soulimane, G. Buse, G.P. Bourenkov, H.D. Bartunik, R. Huber, M.E. Than, Structure and mechanism of the aberrant ba3-cytochrome *c* oxidase from *Thermus thermophilus*, EMBO J. 19 (2000) 1766–1776.
[43] J.P. Collman, R. Boulatov, C.J. Sunderland, L. Fu, Functional analogues of cytochrome *c* oxidase, myoglobin, and hemoglobin, Chem. Rev. 104 (2004) 561–588.
[44] E. Kim, E.E. Chufán, K. Kamaraj, K.D. Karlin, Synthetic models for heme-copper oxidases, Chem. Rev. 104 (2004) 1077–1133.
[45] R. Boulatov, Understanding the reaction that powers this world: biometric studies of respiratory O_2 reduction by cytochrome oxidase, Pure Appl. Chem. 76 (2004) 263–319.
[46] J.G. Liu, Y. Naruta, F. Tani, A functional model of the cytochrome *c* oxidase active site: unique conversion of a heme-μ-peroxo-Cu^{II} intermediate into heme-superoxo/Cu^{I}, Angew. Chem. Int. Ed. 44 (2005) 1836–1840.
[47] T. Chishiro, Y. Shimazaki, F. Tani, Y. Tachi, Y. Naruta, S. Karasawa, S. Hayami, Y. Maeda, Isolation and crystal structure of a peroxo-bridged heme-copper complex, Angew. Chem. Int. Ed. 42 (2003) 2788–2791.
[48] D. del Rio, R. Sarangi, E.E. Chufán, K.D. Karlin, B. Hedman, K.O. Hodgson, E.I. Solomon, Geometric and electronic structure of the heme-peroxo-copper complex [(F8TPP)Fe^{III}-(O_2^{2-})-Cu^{II}(TMPA)](ClO_4), J. Am. Chem. Soc. 127 (2005) 11969–11978.
[49] S. Han, S. Takahashi, D.L. Rousseau, Time dependence of the catalytic intermediates in cytochrome *c* oxidase, J. Biol. Chem. 275 (2000) 1910–1919.
[50] E. Olkhova, V. Helms, H. Michel, Titration behavior of residues at the entrance of the D-pathway of cytochrome *c* oxidase from *Paracoccus denitrificans* investigated by continuum electrostatic calculations, Biophys. J. 89 (2005) 2324–2331.
[51] M. Ruitenberg, A. Kannt, E. Bamberg, B. Ludwig, H. Michel, K. Fendler, Single-electron reduction of the oxidized state is coupled to proton uptake via the K pathway in *Paracoccus denitrificans* cytochrome *c* oxidase, Proc. Natl. Acad. Sci. U. S. A. 97 (2000) 4632–4636.
[52] J. Xu, M.A. Sharpe, L. Qin, S. Ferguson-Miller, G.A. Voth, Storage of an excess proton in the hydrogen-bonded network of the D-pathway of cytochrome *c* oxidase: identification of a protonated water cluster, J. Am. Chem. Soc. 129 (2007) 2910–2913.
[53] D.M. Popović, A.A. Stuchebrukhov, Electrostatic study of the proton pumping mechanism in bovine heart cytochrome *c* oxidase, J. Am. Chem. Soc. 126 (2004) 1858–1871.
[54] W. Humphrey, A. Dalke, K. Schulten, VMD: visual molecular dynamics, J. Mol. Graph. 14 (1996) 33–38.